Micro- and nanoelectronics. Condensed matter physics

Микро- и наноэлектроника. Физика конденсированного состояния

UDC 538.913, 538.958, 538.975
https://doi.org/10.32362/2500-316X-2022-10-3-74-84

RESEARCH ARTICLE

Polarization analysis of THz radiation using a wire grid polarizer and ZnTe crystal

Farkhad A. Zainullin [@], Dinar I. Khusyainov, Marina V. Kozintseva, Arseniy M. Buryakov

MIREA – Russian Technological University, Moscow, 119454 Russia
[@] Corresponding author, e-mail: madflyzero@gmail.com

Abstract

Objectives. Terahertz time domain spectroscopy (THz-TDS) is currently a promising research method in pharmacology and medicine due to the high sensitivity of terahertz radiation to the chemical composition and molecular structure of organic compounds. However, due to the chirality of many biomolecules, their analysis is performed by THz irradiation with circular dichroism. In particular, circular dichroism of THz radiation allows the study of "soft" vibrational movements of biomolecules with different chiralities. Therefore, when studying such biological materials, accurate control of THz radiation parameters is essential. The paper describes a method for characterizing THz radiation polarization on the example of a black phosphorus source material.

Methods. The analysis of polarization parameters of THz radiation experimentally obtained by THz-TDS and using terahertz polarizers was performed by mathematical modeling of the interaction between THz radiation and a ZnTe crystal as a detector.

Results. Two schemes of terahertz spectroscopy with the ZnTe crystal as the detector were discussed in detail. The polarization parameters were determined using one or two wire-grid THz polarizers. An expression for approximating the dependences of the peak-to-peak amplitude of THz radiation on the rotation angle of the wire-grid THz polarizer for these cases was derived. The impact of the terahertz electric field intensity value on the shape of polarization dependences was considered. The rotation angle of the polarization ellipse of THz radiation emitted by the surface of a bulk-layered black phosphorus crystal illuminated by femtosecond laser pulses was determined.

Conclusions. The amplitude of the THz radiation electric field intensity begins to impact the shape of polarization dependences when its value becomes comparable to or exceeds 40 kV/cm.

Keywords: time-resolved terahertz spectroscopy, ellipticity, polarization, electrooptic crystal, electrooptic sampling

• **Submitted:** 21.02.2022 • **Revised:** 13.04.2022 • **Accepted:** 26.04.2022

For citation: Zainullin F.A., Khusyainov D.I., Kozintseva M.V., Buryakov A.M. Polarization analysis of THz radiation using a wire grid polarizer and ZnTe crystal. *Russ. Technol. J.* 2022;10(3):74–84. https://doi.org/10.32362/2500-316X-2022-10-3-74-84

Financial disclosure: The authors have no a financial or property interest in any material or method mentioned.

The authors declare no conflicts of interest.

НАУЧНАЯ СТАТЬЯ

Анализ поляризации ТГц-излучения с помощью решетчатого поляризатора и кристалла ZnTe

Ф.А. Зайнуллин [@], Д.И. Хусяинов, М.В. Козинцева, А.М. Буряков

МИРЭА – Российский технологический университет, Москва, 119454 Россия
[@] Автор для переписки, e-mail: madflyzero@gmail.com

Резюме

Цели. Химический состав и молекулярная структура органических соединений обладают высокой чувствительностью к терагерцовому излучению. Поэтому терагерцовая спектроскопия во временно́й области в настоящее время является перспективным методом исследования в области фармакологии и медицины. Однако из-за того, что многие биомолекулы обладают хиральностью, их анализ проводится путем облучения ТГц-излучением с круговым дихроизмом. В частности, круговой дихроизм ТГц-излучения позволяет исследовать «мягкие» колебательные движения биомолекул с различной закрученностью. Точный контроль параметров этого излучения очень важен при исследовании биологических материалов. Цель работы – описать метод, позволяющий охарактеризовать поляризацию ТГц-излучения на примере использования черного фосфора в качестве источника.

Методы. Анализ параметров поляризации ТГц-излучения, экспериментально полученных методом спектроскопии временно́го разрешения, а также с использованием терагерцовых поляризаторов, проводился путем математического моделирования взаимодействия ТГц-излучения и кристалла ZnTe в качестве детектора.

Результаты. В работе подробно рассмотрены две схемы терагерцовой спектроскопии с кристаллом ZnTe в качестве детектора. Определение параметров поляризации выполнено с использованием одного или двух решетчатых ТГц-поляризаторов. Выведено выражение для аппроксимации зависимостей размаха амплитуды ТГц-излучения от угла поворота решетчатого ТГц-поляризатора для этих случаев. Рассмотрено влияние величины напряженности электрического поля терагерцового излучения на форму поляризационных зависимостей. Определен угол поворота эллипса поляризации ТГц-излучения, испускаемого поверхностью объемного слоистого кристалла черного фосфора при воздействии на него фемтосекундных лазерных импульсов.

Выводы. Амплитуда напряженности электрического поля ТГц-излучения начинает влиять на форму поляризационных зависимостей, когда ее величина становится сравнимой или превышает 40 кВ/см.

Ключевые слова: терагерцовая спектроскопия временно́го разрешения, эллиптичность, поляризация, электрооптический кристалл, электрооптическое стробирование

• **Поступила:** 21.02.2022 • **Доработана:** 13.04.2022 • **Принята к опубликованию:** 26.04.2022

Для цитирования: Зайнуллин Ф.А., Хусяинов Д.И., Козинцева М.В., Буряков А.М. Анализ поляризации ТГц-излучения с помощью решетчатого поляризатора и кристалла ZnTe. *Russ. Technol. J.* 2022;10(3):74–84. https://doi.org/10.32362/2500-316X-2022-10-3-74-84

Прозрачность финансовой деятельности: Авторы не имеют финансовой заинтересованности в представленных материалах или методах.

Авторы заявляют об отсутствии конфликта интересов.

INTRODUCTION

In recent years, the development of time-resolved THz spectroscopy technology has ensured an accurate and simple approach to analyzing material characteristics. Due to the non-ionizing interaction and strong penetrability of THz radiation, additional information on chemical composition or electron–phonon interaction in a sample may be obtained [1–3]. In contrast to infrared (IR) and Raman spectroscopy, THz spectroscopy is very sensitive to the molecular structure and intermolecular interactions in crystals, which is particularly valuable for medical research in pharmacology [4]. In addition, THz radiation excites longer wavelength vibrations, such as phonons in a semiconductor crystal or molecular vibrations in

organic matter, as compared to classical methods of mid-IR spectroscopy and X-ray diffraction. Therefore, it may ensure high reliability in identifying compounds that are difficult to distinguish by other methods [5]. The THz time-domain spectroscopy (THz-TDS) technique is used to analyze materials using THz radiation. This technique is applied to analyzing weak intermolecular interactions, such as lattice vibrations [6], hydrogen bonding [7], Van der Waals interaction [8], as well as collective vibrational modes determined by the molecular configuration, conformation, and general vibration of organic molecules [9]. In particular, THz pulses with elliptically polarized waves are of interest, both in terms of fundamental physics and technological applications. For example, many biomolecules have a chiral structure with rotational/vibrational modes in the terahertz energy range, whose interaction with elliptically polarized THz beams depends on the polarization of THz radiation and chirality of biomolecules. This allows, in particular, the study of "soft" vibrational modes of organic molecules having a different twist [10–12]. Therefore, in order to describe the interaction of THz pulse with the substance, the polarization parameters of THz radiation including ellipticity and rotation direction of the field vector should be obtained [13–15]. The electro-optical sampling technique involving the use of nonlinear optical ZnTe crystal (Russia) as a THz radiation detector in two detection versions based on phase- and amplitude modulation measurements is one of the most common THz-TDS method modifications [16].

Being one of the most promising components of THz devices in the layered semiconductor category, black phosphorus—BP (2dsemiconductors, USA)[1] crystallite was selected as the THz radiation source under study. This is primarily due to the fact that BP represents a "golden mean" between graphene (no bandgap) and semiconducting transition metal dichalcogenides (TMDs), such as molybdenum disulfide (MoS_2), which has a relatively large bandgap of about 2 eV [15]. Moreover, nanoscale films with band gap in the range from 1.5 eV to 0.53 eV may be obtained by varying the number of layers, from one to several [17]. The high carrier mobility of this material (much higher than in TMDs) is also dependent on the number of layers in the range from 299 to 3730 $cm^2/V{\cdot}c$ for electrons and from 337 to 10000 $cm^2/V{\cdot}c$ for holes [18, 19]. This allows THz radiation to be efficiently absorbed even though the photon energy is below the bandgap energy. It is also possible to tune (change) the bandgap width by applying a static electric field [17]. This dynamic bandgap tuning can be used not only to expand the operating wavelength range of BP based devices but also to pave the way for studying electrically tunable topological insulators and semimetals. In this case, the BP crystal allows elliptically polarized THz radiation to be obtained when exposed to linearly polarized femtosecond laser radiation [13].

In the present paper, two versions of polarization analysis of THz radiation are considered in detail. Analyzing in THz-TDS implies two wire-grid polarizers (WGP) used in the first version and one polarizer used in the second one.

METHODS

A variation of the THz-TDS technique allows THz radiation to be detected by electro-optical sampling. Polarization of the laser probe beam is modulated by the THz beam in the electro-optic ZnTe crystal. Using amplitude modulation [16], an optical polarizer crossed with the beam polarization direction is placed on the probe beam path after the ZnTe crystal and before the photodiode (ThorLabs, USA).[2] Under the action of the THz pulse, the beam polarization changes allowing a signal proportional to the amplitude of the THz radiation to be recorded on the diode. The detection method will be described further in more detail.

The electric displacement vector for a homogeneous medium is considered to describe the electro-optic effects in nonlinear optical crystals, as follows:

$$\mathbf{D} = \varepsilon_0 \varepsilon \mathbf{E}, \quad (1)$$

where ε_0 is the electric constant; ε is the dielectric permittivity being a direction-independent scalar quantity; and $\mathbf{E}$ is the electric intensity vector. In the crystal, permittivity may depend on the direction of the electric field relative to the crystallographic axes. In this case, dielectric permittivity is the symmetric tensor while the field $\mathbf{D}$ is generally not parallel to the electric field. Major axes may be transformed into the orthogonal coordinate system wherein $\mathbf{E}$ and $\mathbf{D}$ are related through a diagonal matrix, as follows:

$$\begin{pmatrix} D_1 \\ D_2 \\ D_3 \end{pmatrix} = \varepsilon_0 \begin{pmatrix} \varepsilon_1 & 0 & 0 \\ 0 & \varepsilon_2 & 0 \\ 0 & 0 & \varepsilon_3 \end{pmatrix} \cdot \begin{pmatrix} E_1 \\ E_2 \\ E_3 \end{pmatrix}. \quad (2)$$

Should diagonal elements ε_i be not all the same, as occurs in $CaCO_3$ [20], the crystal exhibits birefringence.

The energy density of the electric field is $\omega_e = \frac{1}{2}\mathbf{E} \cdot \mathbf{D}$. Using matrix (2), it may be shown that surfaces with constant energy density are ellipsoids in field $\mathbf{D}$, written as follows:

[1] https://www.2dsemiconductors.com. Accessed December 22, 2019.

[2] https://www.thorlabs.com. Accessed December 22, 2019.

$$\varepsilon_0\omega_e = \mathbf{D}\cdot\hat{\varepsilon}^{-1}\cdot\mathbf{D} = \frac{D_1^2}{\varepsilon_1}+\frac{D_2^2}{\varepsilon_2}+\frac{D_3^2}{\varepsilon_3}. \quad (3)$$

Introducing non-dimensional vector **u** along direction **D** according to formula $\mathbf{u} = \frac{\mathbf{D}}{\sqrt{2\varepsilon_0\omega_e}}$, the following refractive index ellipsoid equation may be derived:

$$\frac{u_1^2}{n_1^2}+\frac{u_2^2}{n_2^2}+\frac{u_3^2}{n_3^2}=1, \quad (4)$$

where $n_i = \sqrt{\varepsilon_i}$ for a non-magnetic material. The impermeability tensor may be defined as follows:

$$\hat{\boldsymbol{\eta}} = \hat{\varepsilon}^{-1}. \quad (5)$$

Using formula (5), equation (3) may be converted to the following ellipsoid equation:

$$\mathbf{u}\cdot\hat{\boldsymbol{\eta}}\cdot\mathbf{u}=1. \quad (6)$$

Zinc telluride, which has a cubic crystal lattice, is optically isotropic in the absence of the applied electric field. This implies the possibility of replacing the permeability tensor by scalar ε^{-1} multiplied by unit matrix **I**. In the presence of the electric field, the impermeability tensor may be written as follows:

$$\hat{\boldsymbol{\eta}}(\mathbf{E}) = \varepsilon^{-1}\cdot\mathbf{I}+\mathbf{r}\cdot\mathbf{E}. \quad (7)$$

The second term (7) is described by the Pockels effect, where **r** is the tensor of electro-optic coefficients. The electro-optic Kerr effect being quadratic in the electric field may be neglected here, since it is negligible in ZnTe crystal as compared to the linear effect. Thus, having substituted (7) into equation (6), the ellipsoid equation can be written as follows:

$$\mathbf{u}\cdot\hat{\boldsymbol{\eta}}(\mathbf{E})\cdot\mathbf{u} = $$

$$= \sum_{i,j=1,2,3}\left(\varepsilon^{-1}\cdot\delta_{ij}+\sum_{k=1,2,3} r_{ijk}E_k\right)\mathbf{u}_i\mathbf{u}_j = 1. \quad (8)$$

Since tensor $\hat{\boldsymbol{\eta}}$ is symmetric, $r_{ijk} = r_{jik}$. It is conventional to replace the first two indices i, j of tensor **r** by a single index, as follows:

$$r_{11k}\rightarrow r_{1k},$$

$$r_{22k}\rightarrow r_{2k},$$

$$r_{33k}\rightarrow r_{3k},$$

$$r_{23k} = r_{32k}\rightarrow r_{4k},$$

$$r_{13k} = r_{31k}\rightarrow r_{5k},$$

$$r_{12k} = r_{21k}\rightarrow r_{6k}.$$

Zinc telluride crystallizes in the zincblende structure (zincblende comprises two face-centered cubic lattices shifted relative to each other by a quarter of the space diagonal) [21]. In the absence of the applied electric field, the refractive indices are equal, i.e., $n_1 = n_2 = n_3 = n_0$. In addition, **r** contains only one independent non-zero element $r_{41} = r_{52} = r_{63}$. Thus, ellipsoid equation (8) may be written in the following way:

$$\frac{1}{n_0^2}\left(u_1^2+u_2^2+u_3^2\right)+$$

$$+\,2r_{41}\left(E_1u_2u_3+E_2u_3u_1+E_3u_1u_2\right)=1. \quad (9)$$

The ZnTe crystals used for detecting THz radiation have a crystallographic cut (1 1 0), as shown in Fig. 1. Since the THz pulse and the laser pulse fall perpendicular to this plane along the direction [−1 −1 0], their electric vectors lie in plane (1 1 0). The two-dimensional coordinate system (*X, Y*) is introduced in this plane in such a way that *X*-direction coincides with direction [−1 1 0] and *Y*-direction coincides with direction [0 0 1].

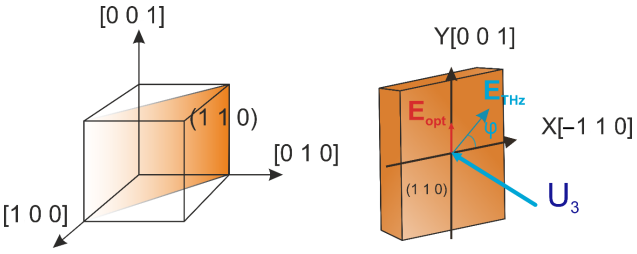

Fig. 1. Plane (1 1 0) (left) and coordinate system (*X, Y*) in this plane (right). The femtosecond laser probe pulse and the THz pump pulse are directed along vector $\mathbf{U_3}$ being the normal to plane (1 1 0)

Major axes should be transformed to obtain the refractive indices in the *XY* plane when applying the electric field.

Let the electric vector $\mathbf{E_{THz}}$ of THz pulse makes angle φ with the *X*-axis (axis [−1 1 0] of ZnTe crystal). Its components in the basis system of the cubic crystal lattice may be represented as follows:

$$\mathbf{E_{THz}} = E_{\mathrm{THz}}\begin{pmatrix}-\cos\varphi/\sqrt{2}\\ \cos\varphi/\sqrt{2}\\ \sin\varphi\end{pmatrix}. \quad (10)$$

In this case, equation (9) is written in the following way:

$$\mathbf{u}\cdot\hat{\boldsymbol{\eta}}\left(\mathbf{E_{THz}}\right)\cdot\mathbf{u}=1,$$

where $\hat{\boldsymbol{\eta}}(\mathbf{E_{THz}})$ is the impermeability tensor depending on field $\mathbf{E_{THz}}$, written in the following way:

$$\hat{\boldsymbol{\eta}}(\mathbf{E_{THz}})=\frac{1}{n_0^2}\begin{pmatrix}1&0&0\\0&1&0\\0&0&1\end{pmatrix}+$$

$$+\,r_{41}E_{\mathrm{THz}}\begin{pmatrix}0&\sin\varphi&\cos\varphi/\sqrt{2}\\\sin\varphi&0&-\cos\varphi/\sqrt{2}\\\cos\varphi/\sqrt{2}&-\cos\varphi/\sqrt{2}&0\end{pmatrix}. \quad (11)$$

Then, the eigenvalues for tensor $\hat{\boldsymbol{\eta}}(\mathbf{E_{THz}})$ may be found from formula (11) in the following way:

$$\lambda_{1,2}=\frac{1}{n_0^2}-\frac{r_{41}E_{\mathrm{THz}}}{2}\left(\sin\varphi\pm\sqrt{1+3\cos^2\varphi}\right),$$

$$\lambda_3=\frac{1}{n_0^2}+r_{41}E_{\mathrm{THz}}\sin\varphi. \quad (12)$$

In this case, the normalized eigenvectors may be written as follows:

$$\mathbf{U_1}=\frac{1}{2}\sqrt{1+\frac{\sin\varphi}{\sqrt{1+3\cos^2\varphi}}}\begin{pmatrix}-1\\1\\2\sqrt{2}\cos\varphi\Big/\left(\sqrt{1+3\cos^2\varphi}+\sin\varphi\right)\end{pmatrix},$$

$$\mathbf{U_2}=\frac{1}{2}\sqrt{1-\frac{\sin\varphi}{\sqrt{1+3\cos^2\varphi}}}\begin{pmatrix}-1\\1\\2\sqrt{2}\cos\varphi\Big/\left(\sqrt{1+3\cos^2\varphi}-\sin\varphi\right)\end{pmatrix},$$

$$\mathbf{U_3}=\frac{1}{\sqrt{2}}\begin{pmatrix}-1\\-1\\0\end{pmatrix}. \quad (13)$$

The directions of major axes coincide with those of the eigenvectors. The refractive indices may be determined by the following formula:

$$n_i=\frac{1}{\sqrt{\lambda_i}}.$$

Considering $r_{41}E_{\mathrm{THz}}\ll\frac{1}{n_0^2}$ the expressions for refractive indices corresponding to major axes may be written as follows:

$$n_1=n_0+\frac{n_0^3r_{41}E_{\mathrm{THz}}}{4}\left(\sin\varphi+\sqrt{1+3\cos^2\varphi}\right),$$

$$n_2=n_0+\frac{n_0^3r_{41}E_{\mathrm{THz}}}{4}\left(\sin\varphi-\sqrt{1+3\cos^2\varphi}\right), \quad (14)$$

$$n_3=n_0-\frac{n_0^3r_{41}E_{\mathrm{THz}}}{2}\sin\varphi.$$

It is clear (Fig. 1, direction $\mathbf{U_3}$) from equation (13) that the third major axis is perpendicular to the crystal plane (1 1 0). This direction coincides with the direction of the THz pump pulse and probe beam pulse propagation. Vector $\mathbf{U_1}$ lies in plane (1 1 0) forming angle ψ with the X-axis [−1 1 0], which can be calculated using the scalar product of vector $\mathbf{U_1}$ and the unit vector along the X-axis. Using the relation $\cos(2\psi)=2\cos^2\psi-1$, the following expression relating angle ψ and angle φ of THz polarization may be written:

$$\cos(2\psi)=\frac{\sin\varphi}{\sqrt{1+3\cos^2\varphi}}. \quad (15)$$

For $\varphi=\pi/2$, major axis U_1 is X-directed while axis U_2 is Y-directed. Therefore, when the electric field is applied to the ZnTe crystal (THz radiation), a refractive index ellipsoid having an ellipse in the XY section is formed (Fig. 2). The directions of the ellipse major axes correspond to the directions of vectors $\mathbf{U_1}$ and $\mathbf{U_2}$. The refractive indices are n_1 and n_2, and correspond to the first two major axes. The larger index (n_s) corresponds to the slower speed of light while the smaller one (n_f) corresponds to the faster speed. The refractive indices are generally denoted by $n_s=n_1$ and $n_f=n_2$.

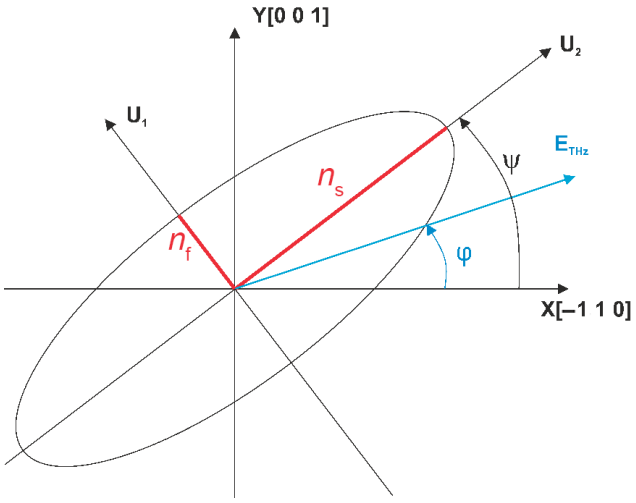

Fig. 2. Refractive index ellipsoid projected onto plane (1 1 0) of ZnTe crystal

The electric intensity vector $\mathbf{E_{THz}}$ makes angle φ with the *X*-axis = [−1 1 0] of ZnTe crystal, while the angle between the semi-major axis of the ellipse and the *X*-axis is ψ(φ). The THz pulse as well as the laser beam falls along the normal to plane (1 1 0) determined by unit vector $\mathbf{U_3} = \frac{1}{\sqrt{2}}\begin{pmatrix}-1\\-1\\0\end{pmatrix}$.

Since the laser beam falls on ZnTe crystal along the direction [−1 −1 0] (eigenvector $\mathbf{U_3}$), its electric vector $\mathbf{E_{opt}}$ lies in plane (1 1 0). In the crystal of thickness *d*, two $\mathbf{E_{opt}}$ components along major axes U_1 and U_2 have a relative phase shift written as follows:

$$\Gamma(\varphi) = \frac{\omega d}{2c} n_0^3 r_{41} E_{\mathrm{THz}} \sqrt{1+3\cos^2\varphi}, \qquad (16)$$

where ω is the angular frequency of laser radiation, φ is the angle between $\mathbf{E_{THz}}$ and the *X*-axis, *d* is the ZnTe crystal thickness, and c is the speed of light.

The signal recorded by the photodiode may be described using the Jones matrix describing the linearly polarized laser beam passing through the birefringent crystal with an optical polarizer [22]. The *S*-polarized laser radiation may be described by the vector as follows:

$$\mathbf{E_{opt}} = E_{\mathrm{opt}}\begin{pmatrix}0\\1\end{pmatrix}, \qquad (17)$$

where E_{opt} is the electric intensity of the laser probe beam. The polarization plane rotation by the angle ψ may be described by the matrix in the following way:

$$R(\psi) = \begin{pmatrix}\cos\psi & \sin\psi\\ -\sin\psi & \cos\psi\end{pmatrix}, \qquad (18)$$

where $\psi = \frac{1}{2}\arccos\left[\frac{\sin\varphi}{\sqrt{1+3\cos^2\varphi}}\right]$ is the rotation angle of the beam polarization ellipse in ZnTe under the THz pulse action.

The birefringence matrix for ZnTe crystal may be written as follows:

$$\mathbf{Z(\varphi)} = \begin{pmatrix}\exp(-i\Gamma(\varphi)/2) & 0\\ 0 & \exp(i\Gamma(\varphi)/2)\end{pmatrix}. \qquad (19)$$

The ZnTe impact on the probe beam may be written in the following form:

$$E_{\mathrm{opt}} R(-\psi) Z(\varphi) R(\psi)\begin{pmatrix}0\\1\end{pmatrix}.$$

Having passed ZnTe and the optical polarizer, the electric intensity of the probe beam may be described by the following formula:

$$E = (1 \quad 0)\, E_{\mathrm{opt}} R(-\psi) Z(\varphi) R(\psi)\begin{pmatrix}0\\1\end{pmatrix}.$$

The signal picked up by the photodiode is equal to the following expression:

$$S_x(\varphi) = K \cdot E_{\mathrm{opt}}^2 \sin^2\left(2\psi(\varphi)\right)\sin^2\left(\frac{\Gamma(\varphi)}{2}\right), \qquad (20)$$

where *K* is the photodiode optoelectronic conversion.

Expressing $\sin^2(2\psi(\varphi)) = 1 - \cos^2(2\psi(\varphi))$ and substituting expressions (15) and (16) in (20), the resulting expression for approximation may be written as follows:

$$S_x(\varphi) = K \cdot E_{\mathrm{opt}}^2\left(1 - \frac{\sin^2\varphi}{1+3\cos^2\varphi}\right)\times$$
$$\times \sin^2\left(\frac{(\omega d/2c) n_0^3 r_{41} E_{\mathrm{THz}}\sqrt{1+3\cos^2\varphi}}{2}\right). \qquad (21)$$

RESULTS AND DISCUSSION

In the study, the traditional THz-TDS experimental setup shown in Fig. 3 is used to determine polarization of THz radiation. A femtosecond titanium-sapphire laser with regenerative amplifier generating optical pulses, having a repetition frequency of 3 kHz, duration of 35 fs and central wavelength of 800 nm, is used as the laser source (Avesta Project, Russia).[3] The output optical beam is divided into a pump beam and a probe beam. The pump beam is focused on the BP crystallite surface at the angle of 45°, while the density of optical radiation on the sample surface is about 1 mJ/cm^2. The generated THz radiation is collimated by the parabolic mirror. Passing through two wire grid polarizers—WGPs (Specac Ltd, Great Britain),[4] the THz radiation is focused on the nonlinear optical ZnTe crystal detector by a parabolic mirror. The probe beam passes through the delay line to be focused onto ZnTe crystal in combination with the THz beam. The passing optical probe beam is recorded by photodiode. The electro-optic method based on amplitude modulation is used to record THz radiation [16]. The experiment is performed at room temperature.

[3] http://avesta.ru/. Accessed December 22, 2019 (in Russ.).
[4] https://www.specac.com. Accessed December 22, 2019.

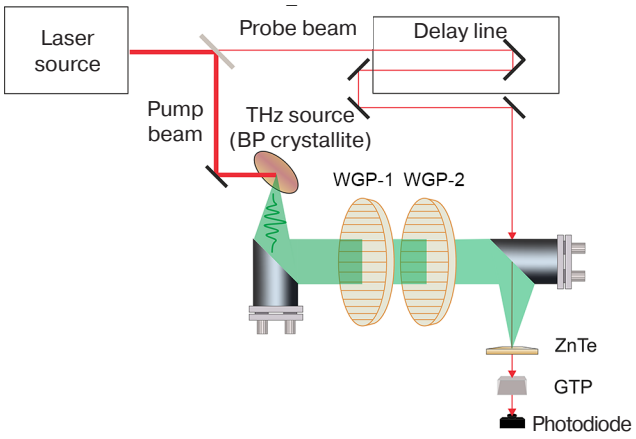

Fig. 3. THz-TDS experimental scheme. GTP is the Glan–Taylor polarizer

The part of the experimental setup responsible for determining the polarization angle of THz radiation is shown in detail in Fig. 4. The angle between the WGP-2 analyzer axis coinciding with vector $\mathbf{E}_{\mathbf{THz}}$, and the X-axis is fixed and equal to φ_3. The WGP-1 polarizer is rotating. The angle between its axis coinciding with vector $\mathbf{E}'_{\mathbf{THz}}$ and the X-axis is φ_2.

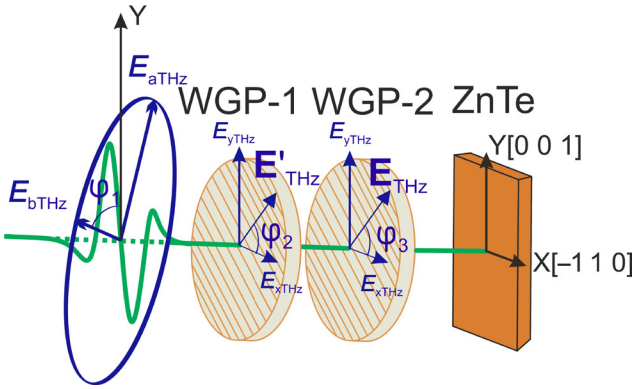

Fig. 4. Experimental setup geometry when using two polarizers

The polarization ellipse of THz radiation lies in a plane parallel to the XY plane. Here, E_{aTHz} and E_{bTHz} are semi-axes of this ellipse; φ_1 is the angle between semi-minor axis and the Y axis; φ_2 and φ_3 are the angles between the X axis and the axes of the WGP-1 and WGP-2 polarizers, respectively.

According to the Malus law, the amplitude of THz radiation may be written in formula (16) in this case as follows:

$$E_{\text{THz}} = E'_{\text{THz}} \cos(\varphi_2 + \varphi_3), \qquad (22)$$

where $E'_{\text{THz}} = E_{\text{aTHz}} \sqrt{\cos^2(\varphi_1 + \varphi_2) + \varepsilon^2 \sin^2(\varphi_1 + \varphi_2)}$ is the THz pulse passed through the first polarizer WGP-1; $\varepsilon = \dfrac{E_{\text{bTHz}}}{E_{\text{aTHz}}}$ is the ellipticity of the pulse under study. Normalizing dependence (21) to the optical beam power taking formula (22) into account and recording the values of angles φ_1 and φ_3, the dependence for the normalized signal $f(\varphi_2)$ recorded by photodiode may be written as follows:

$$f(\varphi_2) = \frac{S_x\left(E_{\text{THz}}(\varphi_1,\varphi_2),\varphi_3\right)}{E_{\text{opt}}^2} = \sin^2(2\psi(\varphi_3))\sin^2\left(\frac{\Gamma\left(E_{\text{THz}}(\varphi_1,\varphi_2),\varphi_3\right)}{2}\right). \qquad (23)$$

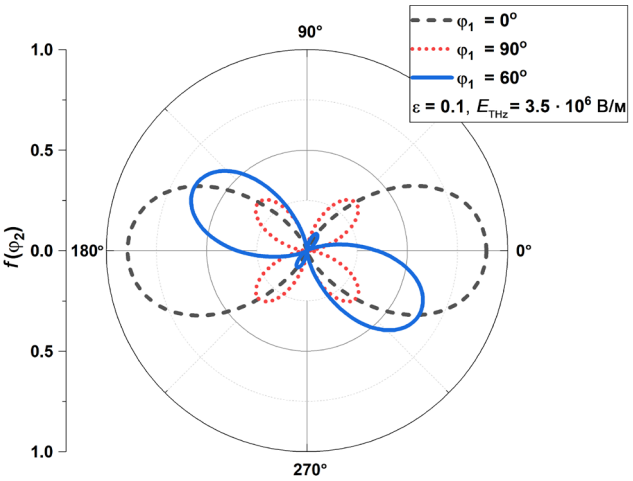

Fig. 5. Dependence plots for the recorded signal normalized to the optical radiation power of the probe beam

The dependence plots $f(\varphi_2)$ derived from expression (23) at different values for THz polarization angles φ_1 are shown in Fig. 5. The remaining parameters of THz radiation and WGP-2 polarizer position are $E_{\text{aTHz}} = 3.5 \cdot 10^6$ V/m; $\varepsilon = 0.1$; and $\varphi_1 = 0°$. Calculating at $\varphi_1 = 0°$ and $\varphi_1 = 90°$, a Dumbbell plot and a four-leaf clover shaped plot are derived, respectively; calculations at other angles, e.g., at $\varphi_1 = 60°$ result in the dependence being shaped transitionally between them. Since dependence $f(\varphi_2)$ is unique for each angle value, the experimental dependence can be easily approximated by expression (23), obtaining the actual parameters of THz radiation (polarization angle, ellipticity).

The smallness condition for the argument of sine $\dfrac{\Gamma(\varphi)}{2}$ is satisfied at $\dfrac{\omega d}{4c} n_0^3 r_{41} E_{\text{aTHz}} \le 0.35$ or at $E_{\text{aTHz}} \le 2 \cdot 10^6$ V/m. Since $\sin^2\left(\dfrac{\Gamma(\varphi)}{2}\right)$ in this case, the polarization dependencies comply with the Malus law when the polarized electromagnetic wave passes through two polarizers. Despite this limitation, the shape of dependences (Fig. 4) does not change up to values $E_{\text{aTHz}} \approx 4 \cdot 10^6$ V/m. When detecting THz wave at

$E_{aTHz} > 4 \cdot 10^6$ V/m, a distortion of the dependencies shown in Fig. 5 is observed. This is due to the phase difference between the ordinary and extraordinary optical beams becoming comparable or exceeding $\pi/2$.

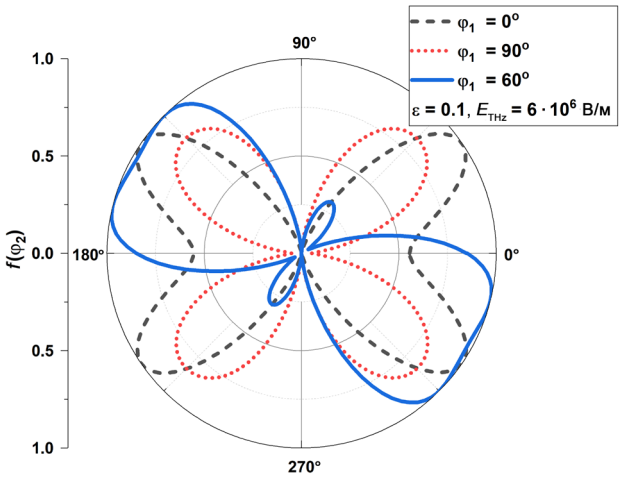

Fig. 6. Dependence plots for the recorded signal of THz pulse passed through two WG polarizers and normalized to the optical radiation power of the probe beam

The dependence plots $f(\varphi_2)$ (23) for $E_{aTHz} = 6 \cdot 10^6$ V/m at different polarization angles of THz radiation φ_1 and for values $\varepsilon = 0.1$, $\varphi_3 = 0$ are shown in Fig. 6. The shapes of dependencies begin to change significantly with increased amplitude of THz radiation. Thus, when $E_{aTHz} = 6 \cdot 10^6$ V/m, dependence $f(\varphi_2)$ is butterfly shaped at $\varphi_1 = 0°$ and four-leaf clover shaped at $\varphi_1 = 90°$ as in the case described above but with maximum values of the function being already comparable with those at the dependence at $\varphi_1 = 0°$; at other φ_1 values, there would be a transitional shape between "butterfly" and "clover."

We shall consider the experimental setup for analyzing THz radiation with one THz polarizer. Since the ZnTe crystal is sensitive to the THz pulse polarization, it could be simultaneously used as the polarization analyzer (Fig. 7).

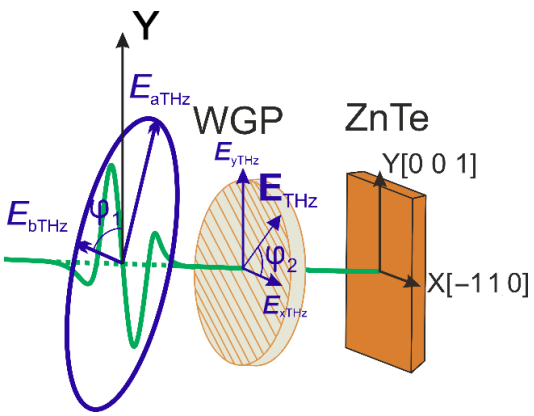

Fig. 7. Experimental setup geometry when using one polarizer

The polarization ellipse of THz radiation lies in the plane parallel to the XY plane. Here, E_{aTHz} and E_{bTHz} are semi-axes of the ellipse; φ_1 is the angle between semi-minor axis and the Y-axis; φ_2 is the angle between the X-axis and the polarizer axis.

In this case, the amplitude of the THz pulse passing through the WGP polarizer may be written in equation (16) in the following form:

$$E_{THz} = E_{aTHz}\sqrt{\cos^2(\varphi_1 + \varphi_2) + \varepsilon^2 \sin^2(\varphi_1 + \varphi_2)}. \quad (24)$$

Normalizing dependence (21) to the optical beam power, considering expression (24) and having the value for angle φ_1 recorded, dependencies $g(\varphi_2)$ at different polarization angles for the THz radiation under study similar in shape to previously derived dependencies (23) may be derived (Fig. 8) as follows:

$$g(\varphi_2) = \frac{S_x\left(E_{THz}(\varphi_1), \varphi_2\right)}{E_{opt}^2} =$$

$$= \sin^2\left(2\psi(\varphi_2)\right)\sin^2\left(\frac{\Gamma\left(E_{THz}(\varphi_1), \varphi_2\right)}{2}\right). \quad (25)$$

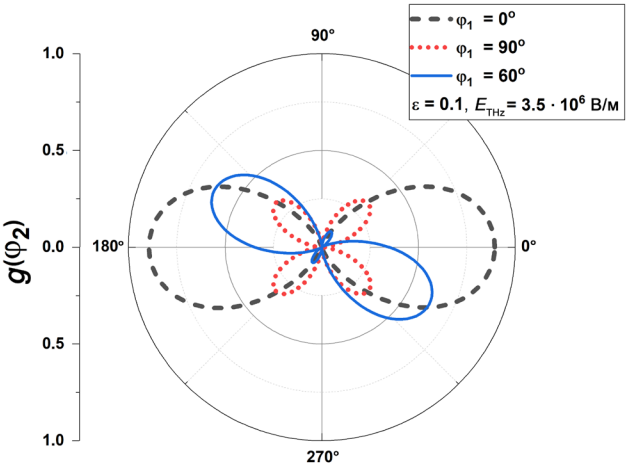

Fig. 8. Dependence plots for the recorded signal of THz pulse passed through WG polarizer and normalized to the optical radiation power of the probe beam

Dependence plots $g(\varphi_2)$ (25) at $E_{aTHz} = 3.5 \cdot 10^6$ V/m, different polarization angles of THz radiation φ_1 and $\varepsilon = 0.1$ are shown in Fig. 8. The plots coincide in shape with dependence plots (23) shown in Fig. 5, which indicates the possibility to analyze the polarization of THz radiation using one WGP. Should the electric intensity value E_{aTHz} exceed $4 \cdot 10^6$ V/m, the change in dependences (25) is observed, as in the case described above.

The BP crystallite used as the THz radiation source in the study has a radiation ellipticity of $\varepsilon = 0.77$ at the fixed angle of 90° between the field vector of the exciting

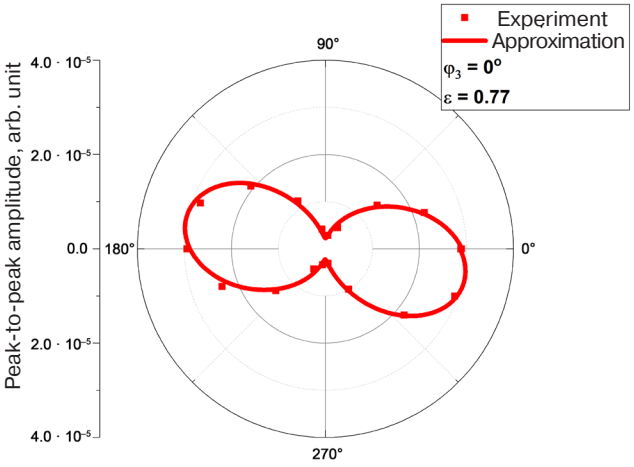

Fig. 9. Dependence plot of the THz peak-to-peak amplitude on the rotation angle of the WGP-1 polarizer

laser pump beam and the sample "zigzag" direction [13]. For analyzing the polarization, a scheme with two wire-grid polarizers is chosen (Fig. 4). The angle φ_3 for WGP-2 is fixed and equal to 0°. The resulting values for the recorded THz peak-to-peak amplitude at different WGP-1 polarizer axis angles φ_3 are shown in Fig. 9 along with the approximation of experimental data by expression (23). Using the approximation, the angle between semi-major axis of the THz polarization ellipse and the *X*-axis has been found to be 40°.

CONCLUSIONS

In the paper, a model describing the dependence of the peak-to-peak amplitude of THz radiation on the rotation angle of the WGP is considered and modified. The simulation results show that the dependences of the THz peak-to-peak amplitude on the polarizer rotation angle are similar in shape whether using two WGPs or one of them in the experimental setup. The possibility of using one polarizer in the analysis due to the ZnTe crystal sensitivity to the polarization of THz radiation is demonstrated. Since, having passed the ZnTe crystal under the THz pulse, the phase difference between the ordinary and extraordinary optical probe beams becomes comparable or exceeds $\pi/2$, dependences begin to differ only with a THz wave field intensity exceeding 40 kV/cm. The applicability of approximation is shown along with the angle $\varphi_1 = 40°$ between the semi-major axis of the THz polarization ellipse, while the *X*-axis is determined by the example of analyzing polarization of THz radiation emitted by the surface of BP crystallite under the femtosecond pump beam action.

ACKNOWLEDGMENTS

The study was supported by the Russian Science Foundation, grant No. 21-79-10353 "Controlled spintronic hybrid THz emitters and detectors." Experimental studies were carried out using the equipment of the Center for Collective Use at the MIREA – Russian Technological University.

Authors' contributions

F.A. Zainullin—mathematical modeling and experimental data processing.
D.I. Khusyainov—experiment.
M.V. Kozintseva—theory.
A.M. Buryakov—theory.

REFERENCES

1. Cui H., Zhang X.B., Yang P., Su J.F., Wei X.Y., Guo Y.H. Spectral characteristic of single layer graphene via terahertz time domain spectroscopy. *Optik* (*Stuttg*). 2015;126(14):1362–1365. https://doi.org/10.1016/j.ijleo.2015.03.032
2. Maamar N., Lazoul M., Latreche F.Y., Trache D., Coutaz J.L. Terahertz time-domain spectroscopy characterization of nitrocellulose in transmission and reflection configurations. *Optik* (*Stuttg*). 2020;224:165711. https://doi.org/10.1016/j.ijleo.2020.165711
3. Tu S., Wang Z., Liang G., Zhang W., Tang Y., She Y., Yi C., Bi X. A novel approach to discriminate transgenic soybean seeds based on terahertz spectroscopy. *Optik* (*Stuttg*). 2021;242:167089. https://doi.org/10.1016/j.ijleo.2021.167089
4. Tan N.Y., Zeitler J.A. Probing phase transitions in simvastatin with terahertz time-domain spectroscopy. *Mol. Pharm.* 2015;12(3):810–815. https://doi.org/10.1021/mp500649q
5. Ho L., Pepper M., Taday P. Signatures and fingerprints. *Nat. Photonics*. 2008;2(9):541–543. https://doi.org/10.1038/nphoton.2008.174
6. Wang W.N., Wang G., Zhang Y. Low-frequency vibrational modes of glutamine. *Chinese Phys. B*. 2011;20(12):123301. https://doi.org/10.1088/1674-1056/20/12/123301
7. Du S.Q., Li H., Xie L., Chen L., Peng Y., Zhu Y.M., Li H., Dong P., Wang J.T. Vibrational frequencies of anti-diabetic drug studied by terahertz time-domain spectroscopy. *Appl. Phys. Lett*. 2012;100(14):143702. https://doi.org/10.1063/1.3700808
8. Andersen J., Heimdal J., Mahler D.W., Nelander B., Wugt Larsen R. Communication: THz absorption spectrum of the CO_2–H_2O complex: Observation and assignment of intermolecular van der Waals vibrations. *J. Chem. Phys.* 2014;140(9):091103. https://doi.org/10.1063/1.4867901
9. Walther M., Plochocka P., Fischer B., Helm H., Uhd Jepsen P. Collective vibrational modes in biological molecules investigated by terahertz time-domain spectroscopy. *Biopolymers*. 2002;67(4–5):310–313. https://doi.org/10.1002/bip.10106
10. Tonouchi M. Cutting-edge terahertz technology. *Nat. Photonics*. 2007;1:97–105. https://doi.org/10.1038/nphoton.2007.3

11. Dadap J.I., Shan J., Heinz T.F. Circularly polarized light in the single-cycle limit: the nature of highly polychromatic radiation of defined polarization. *Opt. Express*. 2009;17(9):7431–7439. https://doi.org/10.1364/OE.17.007431
12. Yang X., Zhao X., Yang K., Liu Y., Liu Y., Fu W., et al. Biomedical applications of terahertz spectroscopy and imaging. *Trends Biotechnol*. 2016;34(10):810–824. https://doi.org/10.1016/j.tibtech.2016.04.008
13. Buryakov A., Zainullin F., Khusyanov D., Abdulaev D., Nozdrin V., Mishina E. Generation of elliptically polarized terahertz radiation from black phosphorus crystallites. *Opt. Eng*. 2021;60(08):082013. https://doi.org/10.1117/1.OE.60.8.082013
14. Khusyainov D., Ovcharenko S., Gaponov M., Buryakov A., Klimov A., Tiercelin N., Pernod P., Nozdrin V., Mishina E., Sigov A., Preobrazhensky V. Polarization control of THz emission using spin-reorientation transition in spintronic heterostructure. *Sci. Rep*. 2021;11(1):697. https://doi.org/10.1038/s41598-020-80781-5
15. Huang Y., Yartsev A., Guan S., Zhu L., Zhao Q., Yao Z., He C.,Zhang L., Bai J., Luo J., Xu X. Hidden spin polarization in the centrosymmetric MoS_2 crystal revealed via elliptically polarized terahertz emission. *Phys. Rev. B*. 2020;102(8):085205. https://doi.org/10.1103/PhysRevB.102.085205
16. Kovalev S.P., Kitaeva G.K. Two alternative approaches to electro-optical detection of terahertz pulses. *JETP Lett*. 2011;94(2):91–96 (in Russ.) https://doi.org/10.1134/S0021364011140074]
[Original Russian Text: Kovalev S.P., Kitaeva G.K. Two alternative approaches to electro-optical detection of terahertz pulses. *Pis'ma v Zhurnal Eksperimental'noi i Teoreticheskoi Fiziki*. 2011;94(2):95–100 (in Russ.).]
17. Deng B., Tran V., Xie Y., Jiang H., Li C., Guo Q., Wang X., Tian H., Koester S. J., Wang H., Cha J. J., Xia Q., Yang L., Xia F. Efficient electrical control of thin-film black phosphorus bandgap. *Nat. Commun*. 2017;8:14474. https://doi.org/10.1038/ncomms14474
18. Long G., Maryenko D., Shen J., Xu S., Hou J., Wu Z., Wong W.K., Han T., Lin J., Cai Y., Lortz R., Wang N. Achieving ultrahigh carrier mobility in two-dimensional hole gas of black phosphorus. *Nano Lett*. 2016;16(12):7768–7773. https://doi.org/10.1021/acs.nanolett.6b03951
19. Chen X., Wu Y., Wu Z., Han Y., Xu S., Wang L., Ye W., Han T., He Y., Cai Y., Wang N. High-quality sandwiched black phosphorus heterostructure and its quantum oscillations. *Nat. Commun*. 2015;6:7315. https://doi.org/10.1038/ncomms8315
20. Hossain F.M., Murch G.E., Belova I.V., Turner B.D. Electronic, optical and bonding properties of $CaCO_3$ calcite. *Solid State Commun*. 2009;149(29–30):1201–1203. https://doi.org/10.1016/j.ssc.2009.04.026
21. Soykan C., Kart S.Ö. Structural, mechanical and electronic properties of ZnTe polymorphs under pressure. *J. Alloys Compd*. 2012;529:148–157. https://doi.org/10.1016/j.jallcom.2012.02.170
22. Yariv A., Yeh P. *Photonics: optical electronics in modern communications*. Oxford University Press; 2007. 836 p.

About the authors

Farkhad A. Zainullin, Intern Researcher, Laboratory "Ultrafast Dynamics in Ferroics," Institute for Advanced Technologies and Industrial Programming, MIREA – Russian Technological University (78, Vernadskogo pr., Moscow, 119454 Russia). E-mail: madflyzero@gmail.com. Scopus Author ID 57226613215, https://orcid.org/0000-0002-1195-5166

Dinar I. Khusyainov, Postgraduate Student, Junior Researcher, Laboratory "Femtosecond Optics for Nanotechnologies," Institute for Advanced Technologies and Industrial Programming, MIREA – Russian Technological University (78, Vernadskogo pr., Moscow, 119454 Russia). E-mail: husyainov@mirea.ru. Scopus Author ID 57194467463, ResearcherID O-7241-2017, https://orcid.org/0000-0003-1332-4146

Marina V. Kozintseva, Cand. Sci. (Phys.-Math.), Assistant Professor, Department of Physics, Institute for Advanced Technologies and Industrial Programming, MIREA – Russian Technological University (78, Vernadskogo pr., Moscow, 119454 Russia). E-mail: kozintseva@mirea.ru. Scopus Author ID 6506049090, ResearcherID C-3826-2017, https://orcid.org/0000-0002-6277-4074

Arseniy M. Buryakov, Cand. Sci. (Phys.-Math.), Senior Researcher, Laboratory "Femtosecond Optics for Nanotechnologies," Institute for Advanced Technologies and Industrial Programming, MIREA – Russian Technological University (78, Vernadskogo pr., Moscow, 119454 Russia). E-mail: buryakov@mirea.ru. Scopus Author ID 55454206600, ResearcherID E-8283-2017, https://orcid.org/0000-0002-3347-9076

Об авторах

Зайнуллин Фархад Алмазович, стажер-исследователь специализированной учебно-научной лаборатории «Сверхбыстрая динамика ферроиков» Института перспективных технологий и индустриального программирования ФГБОУ ВО «МИРЭА – Российский технологический университет» (119454, Россия, Москва, пр-т Вернадского, д. 78). E-mail: madflyzero@gmail.com. Scopus Author ID 57226613215, https://orcid.org/0000-0002-1195-5166

Хусяинов Динар Ильгамович, аспирант, младший научный сотрудник учебно-научной лаборатории фемтосекундной оптики для нанотехнологий Института перспективных технологий и индустриального программирования ФГБОУ ВО «МИРЭА – Российский технологический университет» (119454, Россия, Москва, пр-т Вернадского, д. 78). E-mail: husyainov@mirea.ru. Scopus Author ID 57194467463, ResearcherID O-7241-2017, https://orcid.org/0000-0003-1332-4146

Козинцева Марина Валентиновна, к.ф.-м.н., доцент кафедры физики Института перспективных технологий и индустриального программирования ФГБОУ ВО «МИРЭА – Российский технологический университет» (119454, Россия, Москва, пр-т Вернадского, д. 78). E-mail: kozintseva@mirea.ru. Scopus Author ID 6506049090, ResearcherID C-3826-2017, https://orcid.org/0000-0002-6277-4074

Буряков Арсений Михайлович, к.ф.-м.н., старший научный сотрудник учебно-научной лаборатории фемтосекундной оптики для нанотехнологий Института перспективных технологий и индустриального программирования ФГБОУ ВО «МИРЭА – Российский технологический университет» (119454, Россия, Москва, пр-т Вернадского, д. 78). E-mail: buryakov@mirea.ru. Scopus Author ID 55454206600, ResearcherID E-8283-2017. https://orcid.org/0000-0002-3347-9076

Translated by K. Nazarov
Edited for English language and spelling by Thomas Beavitt